http://dx.doi.org/10.5012/bkcs.2012.33.5.1566

Composite of Indium and Polysorbate 20 as Inhibitor for Zinc Corrosion in Alkaline Solution

Xiaoping Li,[†,§,#] Man Liang,[†,§,#] Hebing Zhou,[‡,§,#] Qiming Huang,[†,§,#] Dongsheng Lv,[†,§,#] and Weishan Li[†,§,#,*]

[†]*School of Chemistry and Environment, South China Normal University, Guangzhou 510006, China.* [*]*E-mail: liwsh@scnu.edu.cn*
[‡]*School of Materials Science and Engineering, South China University of Technology, Guangzhou 510641, China*
[§]*Key Laboratory of Electrochemical Technology on Energy Storage and Power Generation of Guangdong Higher Education Institutes, South China Normal University, Guangzhou 510006, China*
[#]*Engineering Research Center of Materials and Technology for Electrochemical Energy Storage (Ministry of Education), South China Normal University, Guangzhou 510006, China*
Received December 25, 2011, Accepted February 6, 2012

The combined use of indium and polysorbate 20 (Tween 20) was considered as a new inhibition technique for zinc corrosion. Zn and Zn-In alloy coatings were prepared by electrodeposition and their morphology and composition were characterized by scanning electron microscopy (SEM) and inductively coupled plasma atomic emission spectrometry (ICP-AES). The corrosion inhibition effect of indium and Tween 20 on zinc was investigated by polarization curves and electrochemical impedance spectroscopy (EIS). The corrosion inhibition efficiencies obtained from Tafel and EIS analyses are well in agreement. Zinc corrosion can be inhibited to some extent by the individual use of indium and Tween 20 and higher corrosion inhibition efficiency can be obtained by the combined use of indium and Tween 20.

Key Words : Corrosion inhibition, Zinc, Indium, Polysorbate 20

Introduction

Due to its unique merits, low cost, electrochemical reversibility, high specific energy and low equilibrium potential, zinc has been used as the anode materials of primary or secondary batteries.[1-3] The performance of zinc batteries, such as discharge capacity and calendar life, to a great extent depends on the properties of zinc anode. Zinc is active and tends to corrode in alkaline and acidic solution, which causes self-discharge of zinc batteries. Therefore, zinc corrosion should be prevented to develop zinc batteries with high performance.

Conventionally, mercury and its compounds were used as the corrosion inhibitors of zinc anode in zinc batteries because mercury has high hydrogen evolution overpotential. Zinc-mercury alloy is formed when inhibitors containing mercury are used, which inhibits the hydrogen evolution reaction but hardly affects the anodic dissolution of zinc. However, mercury and its compounds have been forbidden to be used in zinc batteries due to the toxicity. Much effort has been made to search for the substitutes for mercury. [4-11]

Indium also has high hydrogen evolution overpotential and has been used as a substitute for mercury in zinc batteries.[12-16] It functions like mercury by forming zinc alloy to inhibit zinc corrosion. Different from mercury, indium inhibits not only the hydrogen evolution reaction but also the zinc dissolution and then affects the discharge performance of zinc batteries. However, indium is a rare metal and expensive.

Several surfactants have been used as substitutes for mercury. The surfactants inhibit zinc corrosion by their adsorption on zinc.[17-19] The polar groups of surfactants are adsorbed on while the non-polar groups escape from the surface of zinc to form a protective layer that inhibits the corrosion of zinc. It has been found that the surfactants containing polyoxyethylene group are more effective than other surfactants as zinc corrosion inhibitors.[20-23] To form a protective layer on zinc, sufficient amount of surfactant needs to be used, which inevitably increases the internal resistance and deteriorates the discharge performance of zinc batteries.

It can be expected that the combined use of indium and surfactant might result in an improved corrosion inhibition for zinc by using less amount of the inhibitors. From this point of view, the combination of indium and a representative polyoxyethylene-based surfactant, polysorbate 20 (Tween 20), was considered as a new inhibition technique for zinc corrosion. The corrosion inhibition efficiencies of zinc by the individual and combined use of indium and Tween 20 were both investigated by using electrochemical methods.

Experimental

Electrodeposition of Zn and Zn-In Alloy. Zn and Zn-In alloy coatings were deposited potentiostatically on the surface of a nickel rod with a purity of 99.999%, respectively. The nickel rod was embedded in an epoxy holder, leaving an exposed surface with a diameter of 2 mm. The solution for Zn coating contained 0.37 M $ZnCl_2$, 0.57 M H_3BO_3 and 2.7 M KCl. The same solution but containing 0.025 M $InCl_3$ was prepared for Zn-In coating. All reagents were of analytical

grade. The electrodeposition was carried out in a three-electrode cell at room temperature. A platinum sheet was used as the counter electrode and a saturated calomel electrode as the reference electrode. The electrodeposition potential was set at −1350 mV and the deposition time was 10 minutes.

Characterization of Zn and Zn-In Alloy Coatings. The surface morphology of Zn and Zn-In coatings was observed by scanning electron microscopy (SEM, JEOL JSM-6380LV, Japan). The composition of Zn and Zn-In alloy was analyzed by inductively coupled plasma atomic emission spectrometry (ICP-AES, IRIS IntrepidXSP, USA).

The adsorption of Tween 20 on Zn and Zn-In was identified by Fourier transform infrared spectroscopy (FTIR, IR Prestige-21, Japan). Before the FTIR measurements, Zn and Zn-In alloy samples were immersed into the neat additive for about 6 hours.

Electrochemical Measurements. All electrochemical measurements were performed with PGSTAT-30 (Autolab, Eco Chemie, Netherlands) in a three-electrode cell at room temperature. The deposited Zn or Zn-In alloy was used as the working electrode. The counter electrode was a platinum sheet with a large surface area and the reference electrode was an Hg/3 M KOH/HgO electrode to which all the potentials in this paper were referred.

The corrosion rate of zinc was evaluated by Tafel and EIS analyses. Tafel plots were obtained in the potential range of −200 to +200 mV vs. the open circuit potential (OCP) at a scan rate of 1 mV s^{-1}. The electrochemical impedance spectroscopy was obtained at −1700 mV from 100 kHz to 0.01 Hz.

The effect of the inhibitors on the anodic and cathodic polarization behavior for zinc corrosion was also tested by a faster potential sweep rate (20 mV/s). The potential altered from the OCP to −2000 mV for cathodic polarization measurement and to −900 mV for anodic polarization measurement.

The adsorption behavior of Tween 20 on Zn and Zn-In electrodes was investigated by differential capacitance curves. The differential capacitance curves were measured at between the OCP to −1700 mV under 1000 Hz.

Results and Discussion

Surface Morphology and Composition of Zn and Zn-In Coatings. Figure 1 presents SEM images of Zn and Zn-In coatings. It can be seen from SEM images that the morphology of Zn-In coating is different from that of Zn; Zn-In coating (Figure 1(b)) has a larger particle size than Zn coating (Figure 1(a)). This indicates that the co-deposition affects the particle size of the coating.

ICP was employed to determine indium content in Zn-In coating. For the determination of indium, the sample was dissolved in 5% HNO_3 solution. The obtained contents of Zn and In ions in the solution are 30.9 ppm and 0.2 ppm, respectively. Therefore, Zn and In have been successfully co-deposited but the content of indium in the coating is small, only 0.64%. The content of indium in Zn-In alloy can be controlled by changing the ratio of zinc and indium ion concentration in the solution. As an inhibitor, the content of indium in the alloy is expected to be as low as possible.

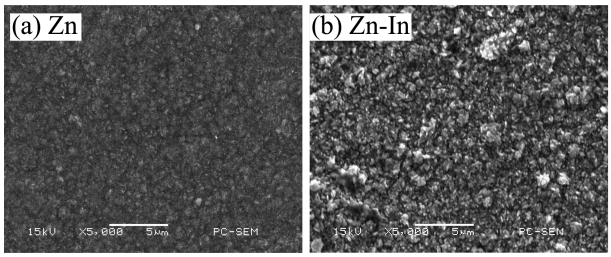

Figure 1. SEM images of (a) Zn and (b) Zn-In coatings.

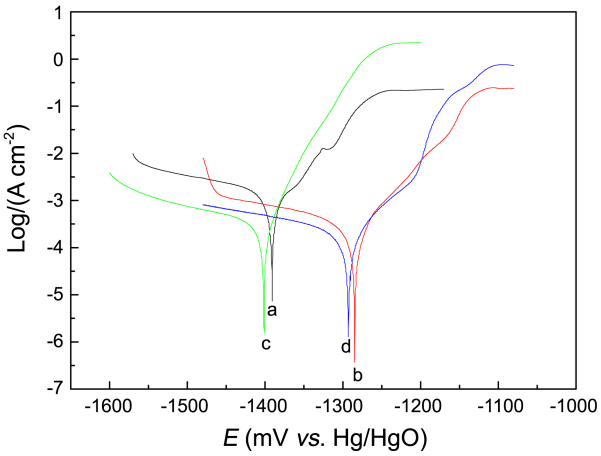

Figure 2. Tafel plots of zinc in 3 M KOH solutions: (a) inhibitor free; (b) indium; (c) Tween 20; (d) indium + Tween 20. Sweep rate: 1 mV/s.

Corrosion Inhibition Efficiency. Figure 2 presents Tafel plots of zinc in 3 M KOH solutions with various inhibitors. The corresponding electrochemical parameters derived from Figure 2 are listed in Table 1. The corrosion current density (I_{corr}) was determined by the extrapolation of the cathodic Tafel curve to the corrosion potential (E_{corr}). It can be seen from Figure 2 and Table 1 that the corrosion potential of zinc shifts negatively by the use of Tween 20 but positively by the use of indium. This suggests that indium affects mainly the anodic process but Tween 20 affects mainly the cathodic process of the zinc corrosion in KOH solution. The corrosion inhibition efficiencies (η_p) of the inhibitors were obtained based on: [24]

$$\eta_p = (I_{corr} - I'_{corr})/I_{corr} \quad (1)$$

Table 1. The electrochemical parameters of zinc derived from the Tafel polarization curves in Figure 3

Inhibitor	E_{corr} (mV)	I_{corr} (mA cm^{-2})	η_p (%)
Free	−1390	1.46	
Indium	−1285	0.49	66.5
Tween 20	−1402	0.38	73.4
Indium + Tween 20	−1293	0.21	85.5

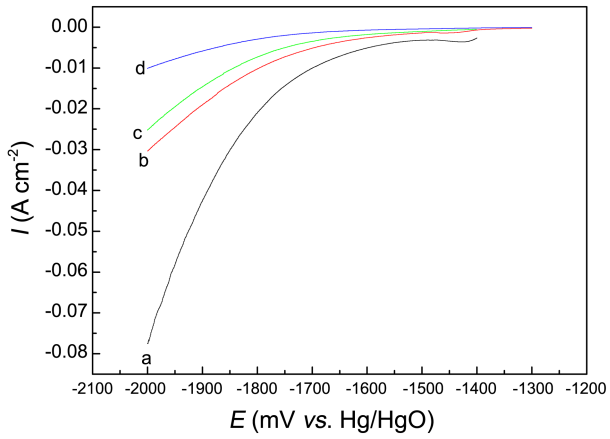

Figure 3. Cathodic polarization curves of zinc in 3 M KOH solutions: (a) inhibitor free; (b) indium; (c) Tween 20; (d) indium + Tween 20. Sweep rate: 20 mV/s.

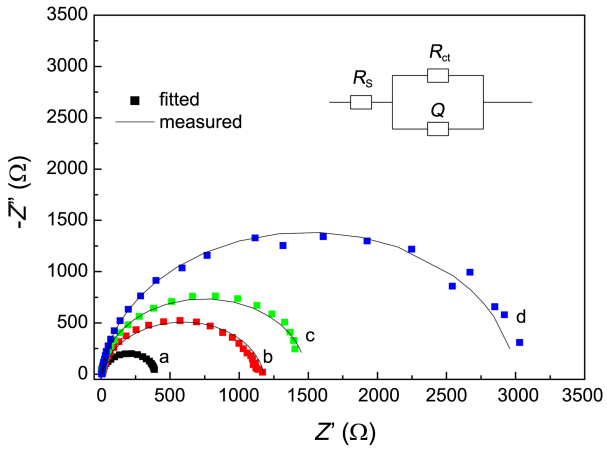

Figure 5. Nyquist plots of zinc in 3 M KOH solutions at hydrogen evolution potential: (a) inhibitor free; (b) indium; (c) Tween 20; (d) indium + Tween 20. The inset is the corresponding equivalent circuit.

where I'_{corr} and I_{corr} are the corrosion current densities of zinc with and without inhibitors, respectively. The inhibition efficiency obtained by the combined use of indium and Tween 20 is 85.5%, higher than those by the individual use of indium (66.5%) and Tween 20 (73.4%). This suggests that there is synergistic effect between indium and Tween 20 for zinc corrosion inhibition.

Figure 3 presents the cathodic polarization curves of zinc with and without inhibitors in 3 M KOH solutions. It can be seen from Figure 3 that the hydrogen evolution reaction on zinc is suppressed to some extent by the individual or combined use of indium and Tween 20. This suggests that all the inhibitors contribute to the corrosion inhibition more or less through the suppression of the cathodic process of zinc corrosion. Tween 20 affects the hydrogen evolution reaction more significantly than indium and the hydrogen evolution reaction is suppressed to a greater extent by the combined use than the individual use of indium and Tween 20.

Figure 4 presents the anodic polarization curves of zinc with and without indium and Tween 20 in 3 M KOH solutions. It can be seen that zinc experiences an active-passive polarization behavior,[25,26] whether the inhibitors are used or not. The open circuit potential of zinc in the solution without using any inhibitor is −1390 mV, but becomes −1285 mV when indium is used. Furthermore, the anodic dissolution current occurs as soon as the potential sweep begins from the open circuit potential for zinc without inhibitor, but does not occurs till −1300 mV when indium is used. The use of Tween 20 hardly affects the open circuit potential and the shape of the anodic polarization curve. The results from anodic polarization curves (Figure 4) and cathodic polarization curves (Figure 3) confirm that indium and Tween 20 play different roles for zinc corrosion inhibition, indium inhibits mainly the anodic process but Tween 20 inhibits the cathodic process of the zinc corrosion in KOH solution.

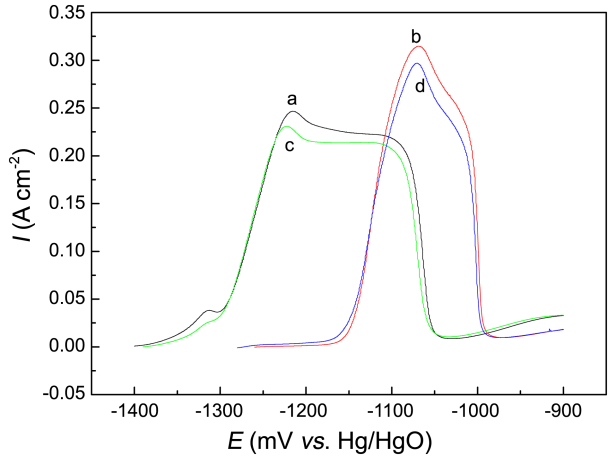

Figure 4. Anodic polarization curves of zinc in 3 M KOH solutions: (a) inhibitor free; (b) indium; (c) Tween 20; (d) indium + Tween 20. Sweep rate: 20 mV/s.

Figure 5 presents the Nyquist plots (dots) of zinc in 3 M KOH solutions at the hydrogen evolution potential. The Nyquist plots are capacitive arcs, indicating that the hydrogen evolution reaction on zinc is controlled by charge transfer step.[27] This reaction can be modeled by a Randles equivalent circuit, as shown by the inset of Figure 5. In the equivalent circuit, R_s represents the solution resistance, R_{ct} represents the charge-transfer resistance and Q is a constant phase element describing the capacitance of the electrode/solution interface. The fitting results by using the equivalent circuit are listed in Table 2.

The corrosion inhibition efficiencies of indium and Tween 20 can be obtained from the charge transfer resistance of Table 2: [28]

$$\eta_R = (R_{ct} - R'_{ct})/R_{ct} \quad (2)$$

where R_{ct} and R'_{ct} are charge transfer resistance of zinc in 3 M KOH solutions with and without inhibitors, respectively. The obtained results are also listed in Table 2. It can be seen that the corrosion inhibition efficiency obtained from EIS, η_R is in a good agreement with that obtained from polarization measurement, η_p. This confirms further the synergistic effect between indium and Tween 20 for zinc corrosion

Table 2. The element parameters for hydrogen evolution reaction on zinc at hydrogen evolution potential

	R_{ct} (Ω)	Q		η_R (%)
		Y_0 (× 10^{-6} s^n Ω^{-1})	n	
Free	394	1.33	0.98	
Indium	1156	4.17	0.91	65.9
Tween 20	1471	3.19	0.97	73.2
Indium + Tween 20	2995	2.06	0.95	86.8

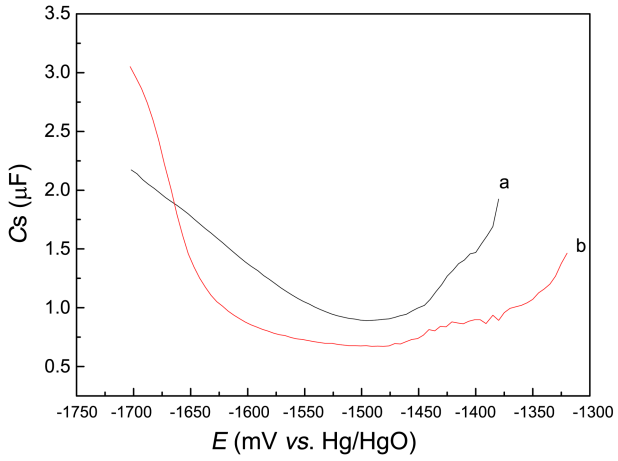

Figure 6. Differential capacitance curves of Zn (a) and Zn-In (b) electrodes in 3 M KOH solutions containing Tween 20.

inhibition.

Adsorption Behavior of the Inhibitor. Figure 6 presents the differential capacitance curves of Zn and Zn-In electrodes in 3 M KOH solutions containing Tween 20. It can be seen from Figure 6 that the capacitance becomes smaller when indium is introduced into zinc, indicating that the adsorption of Tween 20 is preferable on Zn-In electrode to that on Zn electrode. This phenomenon can be explained as follows. As is known that the electron configuration of zinc is [Ar] $4s^2 3d^{10}$ and its outer sub shell is fully filled. While the electron configuration of indium is [Kr] $5s^2 4d^{10} 5p^1$, and there are vacant 5p sub shells to accommodate the unshared electron pairs of oxygen atoms in Tween 20, leading to the preferable adsorption of Tween 20 on Zn-In alloy to that on Zn. The increase of the differential capacitance at the potentials more negative than −1650 mV (*vs.* Hg/HgO) results from the hydrogen evolution reaction.

The adsorption of Tween 20 on Zn and Zn-In alloy can be confirmed by the FTIR experiments. Figure 7 presents the FTIR spectra of Zn-In alloy and Zn after immersion in Tween 20. In the FTIR spectrum of pure Tween 20 (the curve c in Figure 7), the strong peak at 1105 cm^{-1} is characteristic of stretch vibration of -CH_2-O-CH_2- (ν(C-O)), and the broad peak at 3466 cm^{-1} is corresponding to the stretch vibration of hydroxyl group coordinated between molecules by hydrogen bond. The curves of Zn-In alloy (the curve a of Figure 7) and Zn (the curve b of Figure 7) have the same characteristic peaks as the curve c of Figure 7, indicating that Tween 20 has been adsorbed on Zn-In and Zn

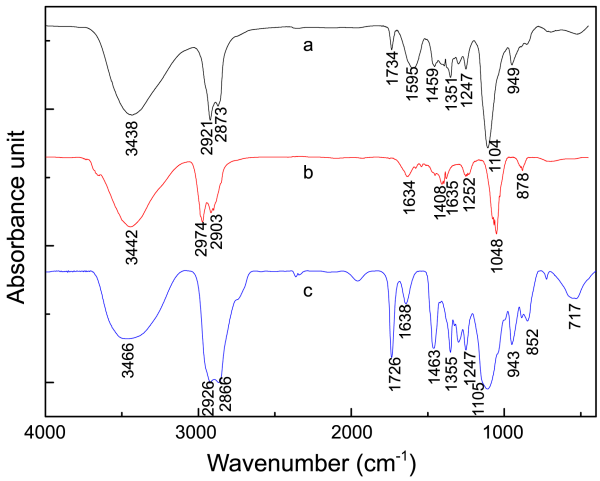

Figure 7. FTIR spectra of Zn-In alloy (a) and Zn (b) after immersion in Tween 20, compared with that of Tween 20 (c).

electrodes. The stronger characteristic peak of Tween 20 on Zn-In at 1104 cm^{-1} than that on Zn at 1048 cm^{-1} confirms a stronger adsorption of Tween 20 on Zn-In alloy than that on Zn. This is the reason why there is a synergistic effect between indium and Tween 20 for zinc corrosion inhibition.

Conclusions

Both indium and Tween 20 can inhibit zinc corrosion in alkaline solution. Indium inhibits zinc corrosion by enhancing simultaneously the overpotential of anodic zinc dissolution and cathodic hydrogen evolution reaction, while Tween 20 by enhancing only the overpotential of the hydrogen evolution reaction. There is a synergistic effect between indium and Tween 20 for zinc corrosion inhibition, because the adsorption of Tween 20 on Zn-In alloy is preferable to that on Zn. This synergistic effect is helpful for reducing the use of indium and Tween 20 in zinc batteries and thus reducing the cost for the manufacture and improving the performance of mercury-free zinc batteries.

Acknowledgments. This work was financially supported by Natural Science Foundation of Guangdong Province (Grant No. 10351063101000001) and Combination Project of Enterprise, University and Scientific Research of Guangdong Province (Grant No. 2011B090400317).

References

1. Coates, D.; Ferreira, E.; Charkey A. *J. Power Sources* **1997**, *65*, 109.
2. Doche, M. L.; Hihn, J. Y.; Touyeras, F.; Lorimer, J. P.; Mason, T. J.; Plattes, M. *Ultrason. Sonochem.* **2001**, *8*, 291.
3. Zhang, X. G. *J. Power Sources* **2006**, *163*, 591.
4. Gagnon, E. G. *J. Electrochem. Soc.* **1986**, *133*, 1989.
5. Jain, R.; Adler, T. C. *J. Appl. Electrochem.* **1992**, *22*, 1039.
6. Li, Q. W.; Liu, R. Q.; Xia, X. *Rare Met.* **1998**, *17*, 145.
7. Binder, L.; Odar, W. *J. Power Sources* **1984**, *13*, 9.
8. Thornton, R. F.; Carlson, E. J. *J. Electrochem. Soc.* **1980**, *127*, 1448.
9. Dzieciuch, M. A.; Gupta, N.; Wroblowa, H. S. *J. Electrochem.*

Soc. **1988**, *135*, 2415.
10. Adler, T. C.; McLarnon, F. R.; Cairns, E. J. *J. Electrochem. Soc.* **1993**, *140*, 289.
11. Zhou, H. B.; Xu, M. Q.; Huang, Q. M.; Cai, Z. P.; Li, W. S. *J. Appl. Electrochem.* **2009**, *39*, 1739.
12. Paramasivam, M.; Jayachandran, M.; Venkatakrishna-Lyer, S. *J. Appl. Electrochem.* **2003**, *33*, 303.
13. Perez, M. G.; O'Keefe, M. J.; O'Keefe, T.; Ludlow, D. *J. Appl. Electrochem.* **2007**, *37*, 225.
14. Zhou, H. B.; Yang, M. Z.; Li, W. S.; Xu, M. Q.; Huang, Q. M.; Hu, S. J. *Rare Metal Mat. Eng.* (in chinese) **2008**, *37*, 404.
15. Cai, Z. P.; Zhou, H. B.; Li, W. S.; Huang, Q. M.; Liang, Y.; Xiao, X. H.; Chen, J. Q. *Rare Metal Mat. Eng.* (in chinese) **2009**, *38*, 1676.
16. Vatsalarani, J.; Geetha, S.; Trivedi, D. C.; Warrier, P. C. *J. Power Sources* **2006**, *158*, 1484.
17. Hu, C. G.; Hu, S. S. *J. Solid State Electrochem.* **2004**, *8*, 947.
18. Dobryszycki, J.; Biallozor, S. *Corros. Sci.* **2001**, *43*, 1309.
19. Wen, D.; Zhu, X.; Zhao, F. Q.; Huang, L. J.; Zeng, B. Z. *J. Solid State Electrochem*. **2006**, *10*, 69.
20. Cohen-Hyams, T.; Ziengerman, Y.; Ein-Eli, Y. *J. Power Sources* **2006**, *157*, 584.
21. Liang, M.; Zhou, H. B.; Huang, Q. M.; Hu, S. J.; Li, W. S. *J. Appl. Electrochem.* **2011**, *41*, 991.
22. Ein-Eli, Y.; Auinat, M.; Starosvetsky, D. *J. Power Sources* **2003**, *114*, 330.
23. Zhou, H. B.; Huang, Q. M.; Liang, M.; Lv, D. S.; Xu, M. Q. *Mater. Chem. Phys.* **2011**, *128*, 214.
24. Fouda, A. S.; Madkour, L. H.; El-Shafel, A. A.; Abd ElMaksoud, S. A. *Bull. Korean Chem. Soc.* **1995**, *16*, 454.
25. Mckubre, M. C. H.; Macdonald, D. D. *J. Electrochem. Soc.* **1981**, *128*, 524.
26. Armstrong, R. D.; Bulman, G. M. *J. Electroanal. Chem.* **1970**, *25*, 121.
27. Wilcox, G. D.; Mitchell, P. J. *J. Power Sources* **1989**, *2*, 345.
28. Ashassi-Sorkhabi, H.; Es'haghi, M. *J. Solid State Electrochem.* **2009**, *13*, 1297.